



TRAPPING TWO-PARTICLE ARRAYS IN A DOUBLE-RING ELECTRODYNAMIC BALANCE

C. L. Aardahl,* R. Vehring,*† E. J. Davis,* G. Schweiger‡ and B. D. Swanson§

*Department of Chemical Engineering, Box 351750, University of Washington, Seattle, WA 98195-1750, U.S.A.

†Ruhr-Universität Bochum, Maschinenbau, Laseranwendungstechnik und Meßsysteme, 44780 Bochum, Germany

§Geophysics Program, Box 351650, University of Washington, Seattle, WA 98195-1650, U.S.A.

(First received 1 August 1996; and in final form 2 January 1997)

Abstract—A new technique has been developed to explore the characteristics and dynamics of the electrodynamic balance (EDB). It is demonstrated that by trapping a pair of microparticles, the electric field of and EDB can be characterized and particle stability can be investigated. The electric field in the neighborhood of the null-point was examined by comparing the oscillatory motion of the two-particle system with a theoretical analysis. In addition, the relevant balance constants were evaluated by five methods: (i) determination of the stabilization strength constant, C_1 , using measurements on two-particle arrays, (ii) determination of the levitation strength constant, C_0 , using measurements on single particles of known mass and charge, (iii) computation of C_1 and C_0 by solving the three-dimensional Laplace equation for the non-axisymmetric electrode system, (iv) computation of C_0 using a ring charge simulation technique, and (v) determination of the ratio C_1/C_0 by measurements of the marginal stability limit. The results of the different methods are compared and shown to be consistent. © 1997 Elsevier Science Ltd. All rights reserved

INTRODUCTION

Electrodynamic containment is one of the principal techniques for manipulating aerosol particles for *in-situ* analysis. The EDB uses ac and dc electric fields to stably trap charged particles. Electrodynamic balances (EDBs) were introduced by Paul and Steinwedel (1953) for the study of atomic ions, but Straubel (1955, 1956) and Wuerker *et al.* (1959) adapted the device to trap microparticles. Although Wuerker *et al.* and Straubel demonstrated trapping and manipulation of clouds of microparticles, interest in this aspect waned, and the EDB became a standard tool for the study of single microparticles. Acoustic levitation of arrays of small charged particles has also been demonstrated (Tian and Apfel, 1996), and Vehring *et al.* (1997) revisited the issue of electrodynamic containment and manipulation of particle clouds, expanding on the analysis of Wuerker and his colleagues to characterize the effects of a dc bias on the compression of particle clouds and to explore particle ejection from a double-ring EDB using a dc bias.

It is highly desirable to be able to chemically characterize particles in the nanometer and submicrometer size ranges, which is currently a difficult task. The EDB makes the measurement of Raman signals possible for particles of order $1\ \mu\text{m}$, and time-of-flight mass spectrometry (TOF-MS) can be performed on even smaller particles. By trapping clouds of aerosol particles and/or using the EDB as an injector for a mass spectrometer, the size range of particles that can be chemically analyzed can be greatly increased.

If an EDB is to be used as a particle injector for a TOF-MS system, a working knowledge of the electric field strength is useful to perform calculations of the forces on trapped particles. The electric field is highly sensitive to the geometry of the electrodes. The field can be calculated using the solution to Laplace's equation, but the solution for a specific geometry can be very tedious, particularly if a three-dimensional field must be computed. Prior to this study, a solution of the field for a non-axisymmetric electrode geometry has not been obtained. An alternate approach is to measure the electric field strength using experimental measurements of particle dynamics. This paper presents new experimental

† Author on leave from Ruhr-Universität Bochum.

methods with which both the ac and dc electric fields can be determined independently, and the experimental results are compared with results based on computations of the three-dimensional electric fields.

THEORY

Electrodynamic trapping

The electrode configuration used in this investigation and the relevant dimensions are presented in Fig. 1. For positively charged particles, the potentials applied to the upper (U) and lower (L) rings are, respectively,

$$V_U = -V_{dc} + V_b + V_{ac} \cos \omega t \quad (1)$$

and

$$V_L = V_{dc} + V_b + V_{ac} \cos \omega t, \quad (2)$$

where $2V_{dc}$ is the dc potential difference between the rings, V_{ac} is the amplitude of the ac field, and V_b is a dc bias voltage which can be applied to both rings to alter the electric field. The circular frequency, ω , is related to the ac frequency, f , by $\omega = 2\pi f$. The bias voltage is usually set equal to zero for particle trapping.

Generally, the dc field is used to balance vertical forces while the ac field acts to focus a charged particle at the null-point of the balance. For a single particle of mass m and charge q , levitated at the mid-plane of the rings, a vertical force balance yields

$$-mg + \sum_i F_i = C_0 \frac{qV_{dc}}{z_0}, \quad (3)$$

where g is the gravitational acceleration, $2z_0$ is the separation distance between the rings, F_i represents vertical forces such as those arising from aerodynamic drag or radiation pressure, and C_0 is the levitation strength constant, which is a geometrical factor that accounts for the deviation of the dc field from the uniform field generated by infinite parallel plates.

The ac field imposes no net force on a particle when it is stabilized at the null-point, but in the neighborhood of the null-point, the radial and axial components of the ac field are proportional to the distance from the null-point. Thus, if more than one particle is trapped, any particles positioned away from the null-point will experience time-dependent forces which are a function of their position in the ac field.

If the particles trapped in the EDB introduce field effects, Poisson's equation must be solved for the potential, but if one assumes that the electric field due to the rings is dominant, Laplace's equation $\nabla^2 \phi = 0$, can be solved for the potential, ϕ . The electric field is related to the potential by $\mathbf{E} = -\nabla \phi$. Several mathematical techniques have been used to determine the electric field of an EDB. Frickel *et al.* (1978) were the first to represent the field of a bihyperboloidal EDB as a series of harmonic polynomials, and Hartung and Avedisian applied this method to develop a generalized form of the equations to account for different electrode geometries. Sloane and Elmoursi (1987) developed a ring charge simulation technique to characterize the electric fields in a bihyperboloidal EDB. Davis *et al.* (1990) applied this ring charge simulation method to develop an approximate solution for the electric fields generated by double rings, and double-ring double-disk EDBs have been analyzed using this method by Davis and Bridges (1994). Recently, Loyalka *et al.* (1995) used a numerical technique based on a Green's function solution for the fields of a representative double-ring geometry. All of this prior work is limited to axisymmetric geometries, neglecting the effect of supporting rods attached to the rings. As we shall show, the presence of supporting rods has some important effects on particle trapping.

The solution of Laplace's equation for the dc field, based on transforming the spherical harmonic solution of the spherical problem to cylindrical (r, z) coordinates, has the form

$$\mathbf{E}_{dc} = V_{dc} \left\{ \left[\frac{3C_2}{z_0^3} zr + \dots \right] \mathbf{e}_r - \left[\frac{C_0}{z_0} + \frac{3C_2}{z_0^3} \left(z^2 - \frac{1}{2} r^2 \right) + \dots \right] \mathbf{e}_z \right\}. \quad (4)$$

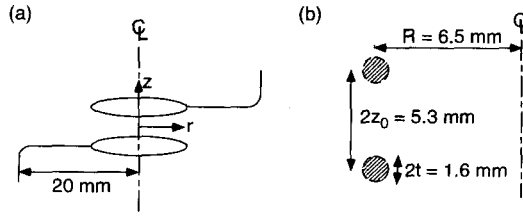


Fig. 1. The electrodes (a) and electrode dimensions (b) used in this study.

Here \mathbf{e}_r and \mathbf{e}_z are unit vectors in the radial and axial directions, respectively, and the coefficients C_0, C_2, \dots are obtained by applying appropriate boundary conditions on the electrodes and surfaces of the bounding chamber. At the center of the EDB ($r = 0, z = 0$), the field corresponds to that used to derive equation (3).

The combined ac and dc bias fields have a structure which can be represented by

$$\begin{aligned} \mathbf{E}_b + \mathbf{E}_{ac} = (V_b + V_{ac} \cos \omega t) & \left\{ \left[\frac{C_1}{z_0^2} r + \frac{3C_3}{z_0^4} \left(2z^2 r - \frac{1}{2} r^3 \right) + \dots \right] \mathbf{e}_r, \right. \\ & \left. - \left[\frac{2C_1}{z_0^2} z + \frac{2C_3}{z_0^4} (2z^3 - 3zr^2) + \dots \right] \mathbf{e}_z \right\}, \end{aligned} \quad (5)$$

where C_1, C_3, \dots are additional coefficients to be determined from the boundary conditions. Hartung and Avedisian called C_1 the stabilization strength constant, and C_0 is the levitation strength constant.

Near the center of the balance, the higher-order terms in equations (4) and (5) can be neglected, and only the constants C_0 and C_1 need be determined to describe the fields. In this approximation, the ac field is linear in r and z . In the experiments and analysis outlined below we shall set $V_b = 0$.

Marginal stability and the equation of motion for a single particle

The marginal stability theory for a single particle trapped at the center of an EDB has been reviewed in detail by Davis (1992); therefore, only a brief overview of the equations need be presented here. The axial stability of a levitated particle is governed by the equation of motion in the z -direction,

$$m \frac{d^2 z}{dt^2} = -mg - qC_0 \frac{V_{dc}}{z_0} + 2C_1 q \frac{(V_{ac} \cos \omega t)}{z_0^2} z - K_d \frac{dz}{dt} + \sum_i F_i, \quad (6)$$

where we have assumed $V_b = 0$. Here, K_d is a drag parameter which, for Stokesian motion of the particle, is given by

$$K_d = 6\pi a \mu / C_c, \quad (7)$$

in which a is the radius of the particle, μ is the velocity of the surrounding gas, and C_c is the Cunningham correction factor (Reist, 1984). When the dc voltage is adjusted so that equation (3) is satisfied, the resulting equation can be transformed to Mathieu's equation (Davis, 1985). The Mathieu equation has been studied extensively, and its stability characteristics are presented by Abramowitz and Stegun (1972). Based on these stability criteria, maps of the stable and unstable regions can be constructed in α - β space, where the parameters α and β are given by

$$\alpha = \frac{6\pi a \mu}{m\omega} \quad \text{and} \quad \beta = \frac{-2g}{z_0 \omega^2} \left(\frac{V_{ac}}{V_{dc}} \right) \left(\frac{C_1}{C_0} \right). \quad (8)$$

The *marginal stability envelope* or set of *springpoints* is defined by the boundaries between stable and unstable regions in the α - β plane. A particle will start to oscillate vertically when

the ac field is changed to cause the particle to move from a stable to an unstable region. Müller (1960) obtained an approximate solution for the lowest portion of the marginal stability curve which is in good agreement with more rigorous solutions of the equation of motion. His solution for the critical value of β , above which instability occurs is,

$$4\beta_{\text{crit}}^2 = \frac{1}{2}(99 + 12\alpha^2) - \sqrt{\frac{1}{4}(99 + 12\alpha^2)^2 - (1 + 4\alpha^2)(81 + 36\alpha^2)}. \quad (9)$$

Here, Müller's original equation has been modified to account for the difference in the definition of β compared with Hartung and Avedisian. Experimentally, β can be varied by changing either the ac amplitude or the ac frequency. Light-scattering data can be used to determine the radius, and for a sphere of known density, ρ , the mass is given by $m = 4\pi\rho a^3/3$. Thus, α can be calculated. When the springpoint is reached, one records V_{ac} , ω , and V_{dc} . The springpoint corresponding to α determines β , and from the definition of β one can calculate the ratio, C_1/C_0 . Therefore, if either C_0 or C_1 can be measured independently, the other coefficient can be determined.

Equation of motion for multiple particles

To investigate the electric field away from the origin, at least two particles must be trapped simultaneously. In that case, the motion of the i th particle is governed by the vector equation of motion (Vehring *et al.*, 1997)

$$m_i \frac{d^2}{dt^2} \mathbf{r}_i + K_{d,i} \left(\frac{d}{dt} \mathbf{r}_i - \mathbf{v}_G \right) = -m_i g \mathbf{e}_z + q_i \mathbf{E}(\mathbf{r}_i, t) + \sum_{j \neq i}^n \frac{q_i q_j (\mathbf{r}_i - \mathbf{r}_j)}{4\pi\epsilon_0 |\mathbf{r}_i - \mathbf{r}_j|^3}. \quad (10)$$

Here, \mathbf{r}_i is the position vector of the i th particle, \mathbf{v}_G is the velocity vector of the surrounding gas, and ϵ_0 is the permittivity of free space. The electric vector $\mathbf{E}(\mathbf{r}_i, t)$ is a superposition of the dc, bias, and ac electric fields:

$$\mathbf{E}(\mathbf{r}, t) = \mathbf{E}_{\text{dc}}(\mathbf{r}) + \mathbf{E}_{\text{b}}(\mathbf{r}) + \mathbf{E}_{\text{ac}}(\mathbf{r}, t). \quad (11)$$

It is useful at this point to decouple the time-dependent small oscillation due the ac field from the large-scale motion which governs the average positions of the particles, \mathbf{r}_i , by writing the approximation (Wuerker *et al.*, 1959; Richardson and Spann, 1984; Arnold and Hessel, 1985; Arnold and Folan, 1987)

$$\mathbf{r}_i = \bar{\mathbf{r}}_i + \mathbf{s}_i(t) = \bar{\mathbf{r}}_i + \delta_i \cos(\omega t + \varphi_i). \quad (12)$$

Here, δ_i is the vector amplitude of the small oscillation and φ_i is the phase shift between the particle motion and the ac drive. By substituting for \mathbf{r}_i and $E(\mathbf{r}, t)$ in equation (10) using equations (11) and (12), the equation of motion reduces to

$$m_i \frac{d^2}{dt^2} \mathbf{s}_i + K_{d,i} \frac{d}{dt} \mathbf{s}_i = q_i \mathbf{E}_{\text{ac}}(\bar{\mathbf{r}}_i, t) = q_i \mathbf{A}_{\text{ac}}(\bar{\mathbf{r}}_i) \cos \omega t, \quad (13)$$

where we have assumed that the gravitational force is balanced by the dc field. Here, \mathbf{A}_{ac} is the amplitude of the ac field at the average radial position of the particle, and \mathbf{A}_{ac} can be obtained from equation (5). Arnold and Hessel solved equation (13), obtaining

$$\delta_i = \frac{q_i \mathbf{A}_{\text{ac}}}{\omega \sqrt{K_{d,i}^2 + m_i^2 \omega^2}} \quad \text{and} \quad \varphi_i = \pi + \tan^{-1} \left(\frac{K_{d,i}}{m_i \omega} \right). \quad (14)$$

In our experiments, the two particles had the same charge and mass, and the dc potential was set to balance the effects of gravity. Equation (5) shows that the field strength in the z -direction is twice that of the r -direction, so the particles are forced into the horizontal plane at $z = 0$ by suitable choice of V_{dc} . This simplifies the analysis, for only the r -direction need be considered to interpret experimental data. Because of their similar charge and mass, the particles repel each other to average radial positions equidistant ($\bar{r}_1 = \bar{r}_2 = \bar{r}$) from the center ($r = 0$). Figure 2 shows how the particles will be positioned for an intermediate (a)- and high (b)-frequency field. At high-frequency the amplitude of oscillation is indiscernable.

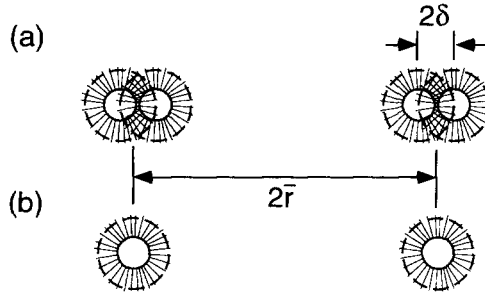


Fig. 2. Particle position and motion for an (a) intermediate and (b) high-frequency electric field.

For the intermediate case, oscillation occurs in the r -direction, and the amplitude of that oscillation is a function of the ac field parameters. Thus, we may write the scalar amplitude

$$\begin{aligned} \delta(\bar{r}) &= \frac{qA_{ac}(\bar{r})}{\omega\sqrt{K_d^2 + m^2\omega^2}} = \frac{qV_{ac}f(\bar{r})}{\omega\sqrt{K_d^2 + m^2\omega^2}} \\ &= \frac{qV_{ac}}{\omega\sqrt{K_d^2 + m^2\omega^2}} = \left(\frac{C_1}{z_0^2}\bar{r} - \frac{3}{2}\frac{C_3}{z_0^4}\bar{r}^3 + \dots \right). \end{aligned} \tag{15}$$

Provided that higher-order terms can be neglected, equation (15) indicates that a graph of measured values of δ as a function of \bar{r} should yield a straight line with slope proportional to C_1 . This makes it possible to measure C_1 .

Force balance

We now determine the equilibrium positions of the particles in the r - θ plane as a function of the electric field settings. Although the relevant equations can be developed for any number of particles, we shall limit the number of particles to two. The force on one of the particles is simply a balance between the repulsive Coulombic force and the attractive force due to the ac field. Thus, a force balance yields

$$\frac{1}{T} \int_0^T qE_{ac}(r, \tau) d\tau + \frac{q^2}{4\pi\epsilon_0(2\bar{r})^2} = 0. \tag{16}$$

Here, the force due to the ac field is averaged over one period, T , of the ac drive. By expanding E_{ac} about \bar{r} in a Taylor series and substituting for \bar{r} using equation (12), we obtain

$$E_{ac}(r, \tau) = E_{ac}(\bar{r}, \tau) + V_{ac}\delta(\bar{r}) \cos(\omega\tau + \varphi) \cos(\omega\tau) \left. \frac{df(r)}{dr} \right|_{\bar{r}}. \tag{17}$$

Integrating the first term in equation (16), substituting for δ using equation (15), and using the results in equation (17), the force balance reduces to

$$f(\bar{r}) \left. \frac{df(r)}{dr} \right|_{\bar{r}} = \frac{\omega\sqrt{K_d^2 + m^2\omega^2}}{8\pi\epsilon_0 \cos \varphi V_{ac}^2 \bar{r}^2} = \frac{C_1^2}{z_0^4}\bar{r} - 6\frac{C_1C_3}{z_0^6}\bar{r}^3 + \dots. \tag{18}$$

Again, we have an independent relationship which can be used to obtain the coefficients of equation (5), for a graph of $f(\bar{r})[df(\bar{r})/d\bar{r}]$ versus \bar{r} should yield a straight line with slope proportional to C_1^2 when the higher-order terms are negligible. However, this relationship is more easily used than equation (15), for the only experimental data needed is the separation distance between the two particles.

EXPERIMENTS

Three types of experiments were performed: (i) experiments on two-particle arrays in which the charge and mass of the particles were known and identical, (ii) experiments on single particles of known charge and mass, and (iii) stability experiments on liquid droplets in which the charge was not known, but the mass could be obtained from light scattering data.

Multiple particle studies

The experimental apparatus has been described in detail by Vehring *et al.* (1997), so only a brief review of the system will be presented here. Solid sodium chloride or sodium sulfate particles were formed by allowing larger aqueous solution droplets to evaporate thereby forming a solid residue. Parent particles were generated using a TSI model 3450 vibrating orifice aerosol generator (VOAG) (Berglund and Liu, 1973), and their charge was regulated using a charging plate (Reischl *et al.*, 1977) which was attached to the VOAG head. The charging plate had a small orifice through which the droplet stream could pass. The induced charge could be altered by varying the potential applied to this plate. The total charge on the droplets which formed upon jet break-up was measured by collecting the particles in a Faraday cup. The Faraday cup was shielded from external stray fields, and the current-to-ground was measured with a Keithley Instruments 610C electrometer. By dividing the current by the frequency of particle generation, the charge on each particle was obtained. Each droplet had a charge between 6.0×10^{-16} and 2.5×10^{-15} C depending on the backing pressure of the VOAG and the potential applied to the charging plate. The mass of the particles was obtained from the VOAG operating parameters using the relationship

$$m = \frac{Q}{f_p} \sum_i c_i M_i, \quad (19)$$

in which Q is the volumetric flow rate of the liquid stream, f_p is the frequency of particle generation, and c_i and M_i are the concentration and molecular weight of species, i , respectively. It is likely that the particles were nearly spherical, so an aerodynamic radius for the particles was estimated by assuming that the particles were non-porous. Based on this assumption, the particles investigated range in radius from 0.8 to 3.9 μm .

The chamber used to house of EDB is depicted in Fig. 3. The particles were allowed to dry in a settling column which was 0.82 m long with a circular cross-sectional area of 7.85×10^{-3} m². Once dried, the particle flow was funneled into the top access port of a stainless-steel chamber which housed the double-ring EDB. The chamber had a volume of 350 ml, and nitrogen gas was passed by the particles at up to 1.5 ml s⁻¹ in order to ensure that the particles were dry.

Often, many particles were trapped, and in this event the ac amplitude was lowered to reduce the number to two particles by destabilizing the other particles. Once two particles were stabilized, photographs of the particles were taken with a SLR camera (Nikon F90) at different ac field settings. The camera was mounted at an angle of 23° from the vertical axis of the balance chamber. A magnification of 1.1 was obtained using a zoom lens (Sigma, 28-70/2.8), a 2X tele-converter, and a 56 mm extension tube. In order to obtain the position of the particles at various field settings, color slides (Kodak Ektachrome Elite 100) were magnified, and calipers were used to determine the particle positions. These measurements were then rescaled by measuring the inner diameter of the rings. The dimensions of interest were the average radial position of each particle and the amplitude of oscillation, the variables appearing in equations (15) and (18).

Similar experiments were done with single levitated particles which were generated in the same fashion as the two-particle arrays. In this case, the dc field was probed rather than the ac field. Because the mass and charge of the particle were known, the levitation strength constant, C_0 , could be obtained from the dc potential required to balance the particle using equation (3).

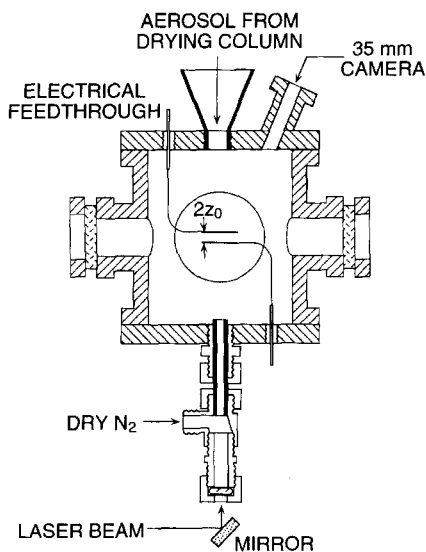


Fig. 3. Front view of the EDB chamber.

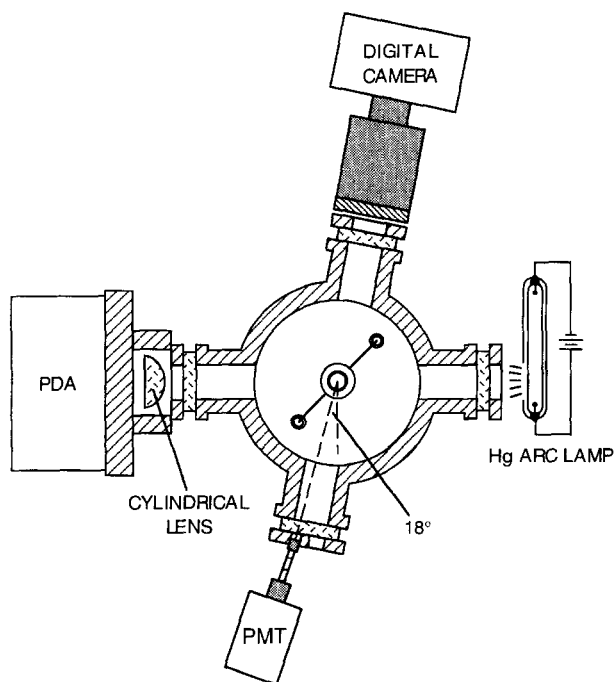


Fig. 4. Top view of the EDB chamber with peripheral equipment.

Stability measurements

To independently validate the results of the measurements on the salt particles, marginal stability measurements were performed on droplets of low vapor pressure esters of phthalic acid, dioctylphthalate (DOP) and dibutylphthalate (DBP). A top view of the EDB and peripherals used to make springpoint measurements is shown in Fig. 4. Droplets ($a \sim 18\text{--}19 \mu\text{m}$) of these materials were trapped in the EDB and springpoints were recorded for various ac frequencies. Then the droplets were exposed to the light from a mercury arc-lamp to remove charges from the particle by photoemission (Arnold and Hessel). After

a significant amount of charge was removed, the springpoints were again measured to obtain additional points on the marginal stability curve.

Droplet radii were measured by comparing angular light scattering data with Mie theory (Bohren and Huffman, 1983). A Texas Instruments TSL 218 photodiode array comprise of 512 photoactive pixels was used to obtain the angular scattering data over the polar angle range $76.3^\circ \leq \theta \leq 104.9^\circ$ at an azimuthal angle of 90° .

RESULTS

The two-particle experiments showed that at high frequencies ($f > 1000$ Hz) particle oscillation was indiscernible. Therefore, a high frequency was used to obtain photographs useful for characterization of the electric field based on equation (18). This method will be called the *point* method because the particles appeared as spots, and the only measurement required is the radial position. At lower frequencies (< 150 Hz) the particle oscillation was too large for the small-oscillation theory to be valid. Therefore, intermediate frequencies (150–400 Hz) were used to obtain amplitude measurements that were believed to satisfy the small-oscillation condition. These data were analyzed using equation (15), and this method will be referred to as the *delta* method.

The particles used in the two-particle experiments were sodium chloride having a mass of 8.7×10^{-15} kg and a charge of 2.5×10^{-15} C. Assuming the spheres to be non-porous, the aerodynamic radius of the particles was estimated to be $a = 0.99 \mu\text{m}$, which yields a drag parameter of $K_d = 3.01 \times 10^{-10} \text{ kg s}^{-1}$.

For measurements using the point method, 18 photographs were taken using an ac frequency of 1006 Hz and an ac voltage that varied over the range 450–1700 V_{rms}. Figure 5 shows a plot of $f(\bar{r})[df(\bar{r})/d\bar{r}]$ versus \bar{r} obtained from the high-frequency experiments. The value of $f(\bar{r})[df(\bar{r})/d\bar{r}]$ can be obtained from the field parameters using equation (18), and based on that relationship there should be a linear correspondence to \bar{r} provided that higher-order terms are negligible. The linear fit shown in Fig. 5 was constrained to pass through the origin in accordance with the form of equation (18). The fit for these high-frequency data yielded a slope of $(2.706 \pm 0.041) \times 10^7 \text{ m}^{-4}$. This corresponds to $C_1 = 0.0365 \pm 0.001$.

Also shown in Fig. 5 are point measurements obtained from lower frequency experiments ($180 < f < 300$ Hz). In this case there was a substantial amplitude of oscillation, so \bar{r} was taken as the mid-point of that oscillation. The slope of the line through these points, constrained to pass through the origin, is $(5.123 \pm 0.073) \times 10^7 \text{ m}^{-4}$, corresponding to $C_1 = 0.050 \pm 0.001$.

This second set of data was also analyzed using the delta method. The specific combination of V_{ac} and ω was adjusted to obtain a similar amplitude of oscillation for each point. Hence, by changing V_{ac} or ω the effect was to change \bar{r} . Thirty-two photographs were taken for various values of the parameters. Figure 6 presents a graph of $f(\bar{r})$ versus \bar{r} based on these experiments. The data are fitted by the straight line with slope $(1.583 \pm 0.083) \times 10^4 \text{ m}^{-2}$. This leads to $C_1 = 0.111 \pm 0.006$, which is substantially larger than the values obtained from the point method.

We should point out that the particles studied were of the order of the wavelength of light. Thus, the optical method used to measure the amplitude of the particle oscillation greatly overestimated the amplitude because of diffraction effects. The scattering efficiency for the salt particles was approximately three. Therefore, the true edge of the particle is obscured by a skirt of light at the particle surface. We have tried to depict this in Fig. 2a which shows the actual size of the particle and its apparent size. By measuring the outer limit of the image obtained photographically the amplitude is overestimated. As a result, C_1 is overestimated. The measurement of the average position of a particle is subject to less error because although the particles appear larger than the actual size, their true radial position is unaffected by diffraction (see Fig. 2b).

Therefore, the delta method is not a good technique for analyzing data at intermediate frequency, and the values of C_1 obtained using the point method should be more reliable.

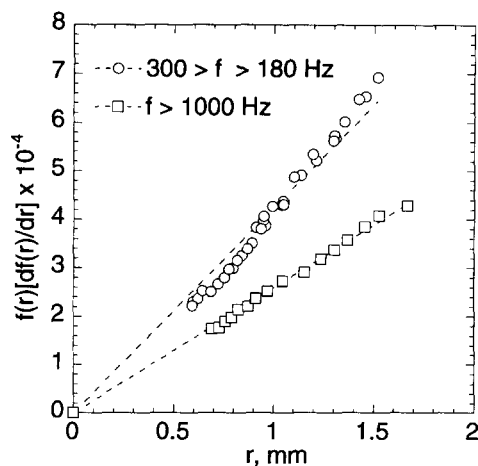


Fig. 5. The particle position data analyzed using the point method.

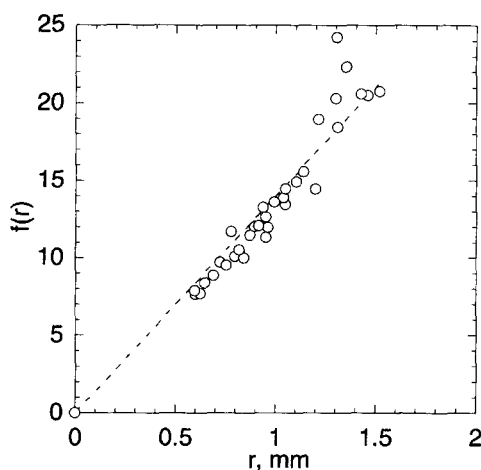


Fig. 6. Intermediate frequency data analyzed using the delta method.

To examine the discrepancy among the two estimates of C_1 using the point method we performed additional measurements. The ratio C_1/C_0 was determined using marginal stability measurements, and C_0 was measured using single particles of independently measured charge and mass.

Marginal stability results

To obtain C_1 via the marginal stability technique, C_0 must be known because β versus α data will only yield the ratio, C_1/C_0 . We obtained C_0 directly from measurement of the dc voltage required to levitate particles of known mass and charge. The apparatus used to generate the two-particle arrays was used in these experiments as well. However, a number of different particles were used to provide a large database for the determination of C_0 . Four different feed solutions (0.013 M NaCl, 0.110 M NaCl, 0.093 M Na₂SO₄, and 0.390 M Na₂SO₄) were used to generate particles of different mass. In addition, the charge on the particles was varied by adjusting the potential applied to the charging plate. Analysis of 33 different particles yielded a value of $C_0 = 0.441 \pm 0.014$.

Figure 7 shows the results of the marginal stability study. Two compounds, DOP and DBP, were used to obtain the data in the figure. The data conform to the theoretical stability limit very well. This agreement was reached by setting $C_1/C_0 = 0.070$ in the

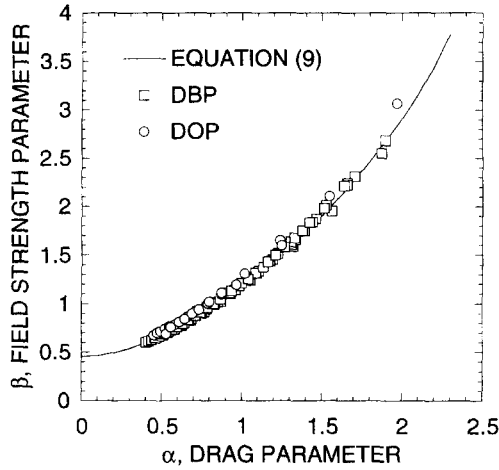


Fig. 7. Marginal stability data compared with theory for $C_1/C_0 = 0.070$.

definition of β . Based on $C_0 = 0.441 \pm 0.014$ the marginal stability results yield $C_1 = 0.031 \pm 0.001$, which is in reasonable agreement with the value 0.0356 obtained from the high-frequency two-particle data.

DISCUSSION

It is apparent from Figs 5 and 6 that the functions $f(r)$ and $f(r)[df(r)/dr]$ are linear functions of \bar{r} . This implies that the cubic term and terms of higher order in equations (15) and (18) are negligible for the range of \bar{r} studied here. This is not surprising for positions closer to the center of the chamber, but it is surprising for the data obtained at $\bar{r} \sim 1.7$ mm. The inner diameter of the rings is only 5.7 mm, so this value of \bar{r} corresponds to a position that is relatively far from the null-point. We were unable to hold particles at radii greater than 1.7 mm, probably due to a decrease in the field beyond that point. This speculation is consistent with the fact that any cubic term which becomes significant, acts to decrease the r -component of the ac field [see equation (5)]. This result also suggests that truncation of the polynomial series after the linear term is valid for $\bar{r}/R \leq 0.3$.

Although the point measurements suffer the least from inaccuracies in the optical measurements, one must have an accurate value of the phase shift to calculate C_1 . The accuracy of φ is related to the value of K_d [equation (14)]. The value of K_d reported above was based on the assumption that the particles were non-porous. As the porosity increases K_d increases, and the value of C_1 calculated from the point measurements increases as well. For example, a voidage of 50% would result in C_1 values of 0.046 and 0.056 for the data of Fig. 5. This is a 20% change in C_1 .

Errors in the phase shift are likely the reason why the lines in Fig. 5 have such a different slope. At intermediate frequency (upper data set) the phase shift is likely different from that predicted by small oscillation theory. Hence, a large value of C_1 is calculated from the slope. As the amplitude of the oscillation increases there is an increasing asymmetry in the Coulombic forces due to the $1/r^2$ dependence. As a result, the motion of the particle is no longer sinusoidal leading to breakdown of the delta method.

Solution of the nonlinear equation of motion

To examine the validity of the point measurements, we solved equation (10) numerically with no constraint of small particle oscillation. For two particles of the same mass and charge, levitated in the $z = 0$ plane, the equation of motion reduces to

$$m \frac{d^2 r}{dt^2} + K_d \frac{dr}{dt} = \frac{qV_{ac}C_1}{z_0^2} r \cos \omega t + \frac{q^2}{16\pi\epsilon_0 r^2}. \quad (20)$$

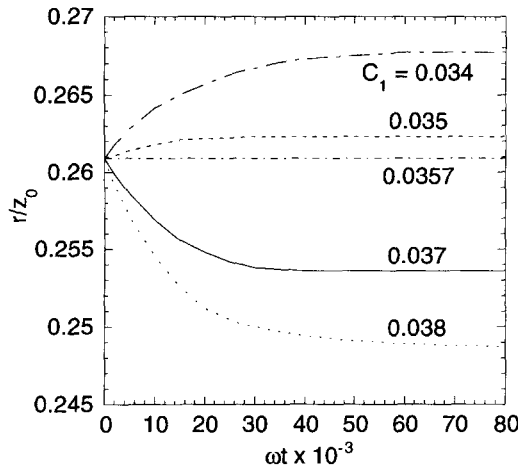


Fig. 8. Solutions of equation (20) for different values of C_1 .

Again it has been assumed that the truncated series for the ac electric field is valid for the region of interest and that the particles do not oscillate vertically. The equation was solved using a fourth-order Runge–Kutta method with initial conditions $r = \bar{r}$ and $dr/dt = 0$ at $t = 0$. The solution yields a time-dependent trajectory which oscillates about \bar{r} with some amplitude that depends on C_1 , V_{ac} , and ω . The mean value \bar{r} approaches a constant value as time increases, and the asymptotic value of \bar{r} is a function of C_1 . If the initial value of \bar{r} is taken to be the asymptotic value corresponding to some specific value of C_1 , \bar{r} will remain at its initial value. For any other value of C_1 , \bar{r} will change in time until a new asymptotic value is reached.

Figure 8 shows how C_1 affects the solution of equation (20). The initial value of \bar{r} corresponds to a measured value from the high-frequency experiments. Notice that if $C_1 = 0.0357$ the solution is quasi-stable; otherwise, \bar{r} drifts away from the measured value. This value of C_1 is in excellent agreement with the value obtained using the point method with high-frequency data.

Another interesting aspect of the solution of equation (20) is shown in Fig. 9. Here, all of the data obtained from the two-particle measurements and the corresponding solutions of equation (20) are plotted versus $-V_{ac} \cos \varphi / \omega$. The high-frequency results of theory and experiment are in excellent agreement, and the theoretical results for intermediate frequencies fall on the same curve. The data obtained at intermediate frequencies fall below the other results by 13%. This suggests that the intermediate frequency data do not satisfy the small oscillation condition. A potentially useful dimensionless group which involves the correlating variable is $qV_{ac} \cos \varphi / K_d z_0^2 \omega$.

Ring-charge simulation

The values of C_0 and C_1 obtained from the experiments incorporate the effects of the supporting rods. The asymmetry introduced by the rods makes it possible to trap arrays of particles that are stationary in the azimuthal direction. This useful result is not possible with a perfectly axisymmetric system. But the rods affect the electric fields in ways that have not been explored. It is informative to compare theoretical values of the coefficients with the experimental results. Davis *et al.* (1990) developed an approximate solution for C_0 for the axisymmetric double-ring electrode configuration based on the ring charge simulation technique. The technique involves placing a number of ring charges on each electrode, obtaining the field generated by the different ring charges by a superposition principle. The analysis scheme of Davis and his coworkers, which used only eight rings in the simulation, should give a reasonable value of C_0 for the small ring separation used here. Their

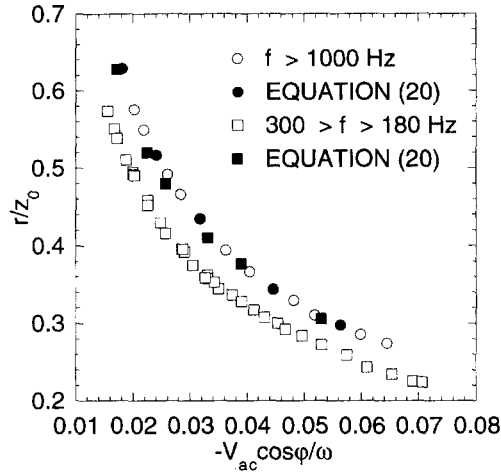


Fig. 9. Correlated data for the average radial position compared with solutions of equation (20).

approximation is

$$C_0 = \frac{\pi z_0^2}{\psi(\xi_1, \xi_2)(R^2 + z_0^2)^{3/2}}, \quad (21)$$

where

$$\psi(\xi_1, \xi_2) = \frac{K(\xi_1)}{2R} + \frac{K(\xi_2)}{2(R^2 + z_0^2)^{1/2}}, \quad (22)$$

and the parameters ξ_1 and ξ_2 are defined by

$$\xi_1 = 1 - \frac{t^2}{4R^2} \quad \text{and} \quad \xi_2 = 1 - \frac{t^2 + 4z_0^2}{4R^2}. \quad (23)$$

Here, $K(\xi_i)$ is the complete elliptic integral of the first kind, and R , t and z_0 are the dimensions shown in Fig. 1b. For the dimensions indicated in Fig. 1b, equation (21) yields $C_0 = 0.410$, which is only 7% lower than the value measured by trapping single particles of known mass and charge.

A better understanding of the effects of the asymmetry on the electric fields can be obtained by solving the three-dimensional Laplace equation, taking into account the support rods and the chamber boundaries.

Solution of Laplace's equation for a non-axisymmetric electrode geometry

The charge simulation technique and the other methods based on axisymmetric electrodes do not allow for distortions in the field due to the rods which hold the rings in place. Therefore, a numerical code was formulated which solved Laplace's equation for the chamber and electrode geometries used in the experiments. The method of relaxation was used with a fine three-dimensional mesh. The procedure started by setting the potential equal to zero everywhere except on the rings and posts which had potentials $V_{ac} = 10$ V and $V_{dc} = 0$, and $V_b = 0$. The ac and dc fields were solved for separately, and the superposition of these fields was taken to be the field that acted on any trapped particles in the EDB. All the chamber walls were kept at ground potential to be consistent with the experimental runs. Using the relaxation algorithm, the potential at each grid point was adjusted until all the points in the mesh satisfied Laplace's equation to within the desired accuracy.

The results of the computation for the ac field are displayed in three-dimensional form in Fig. 10. The ac potential is shown for $\omega t = 0$, that is, at its maximum strength. The influence of the support posts is clearly seen in the two ridges which extend out from the central depression.

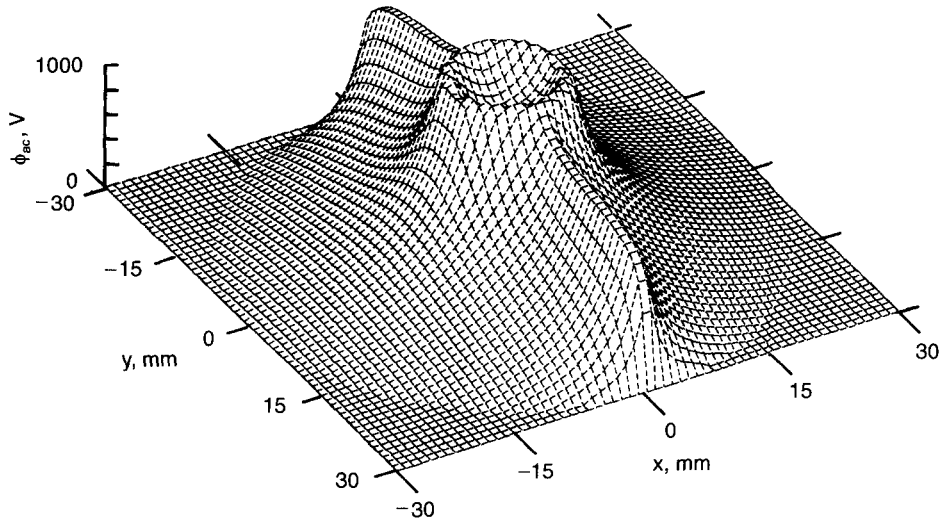


Fig. 10. The ac potential distribution at the midpoint ($z = 0$).

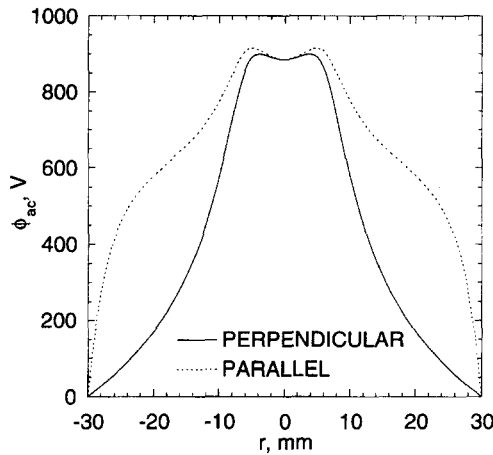


Fig. 11. The ac potential distributions corresponding to Fig. 10 for $\theta = 0^\circ$ (parallel to the plane of the support rods) and $\theta = 90^\circ$ (perpendicular).

A simpler and more useful depiction of the ac field is presented in Fig. 11, which shows the potential at the midplane ($z = 0$) in the plane of the posts ($\theta = 0^\circ$ or \parallel) and in the plane perpendicular to the posts ($\theta = 90^\circ$ or \perp). The distortion of the ac field by the posts is clearly indicated by the bulge in the potential and by the deeper potential well in the center of the chamber for the parallel slice compared with the perpendicular plane. By curve-fitting the data in Fig. 11 and differentiating the resulting function, C_1 is obtained by applying equation (5). This procedure yields $C_{1\parallel} = 0.0428$, and $C_{1\perp} = 0.0317$. The mean value of C_1 (averaged over all θ) should be close to $C_{1\perp}$, for the effects of the rods are limited to a relatively small range of angles near $\theta = 0^\circ$.

A similar numerical procedure applies for the evaluation of C_0 . The three-dimensional dc field at the midplane ($z = 0$) is plotted in Fig. 12 for $V_{ac} = V_b = 0$ and $V_{dc} = 10$ V for the rings and support rods. One can see that the dc potential is an odd function, and again the effects of the support rods are obvious.

By computing the dc potential along the z -axis, C_0 can be determined. Figure 13 shows a plot of the dc potential along the axis of the chamber as a function of z . The slope of the curve at $z = 0$ yields the z -component of the dc field at the center. If this value is normalized by the imposed field ($10/z_0$ V m $^{-1}$ in this case), C_0 is obtained using equation (4). The result

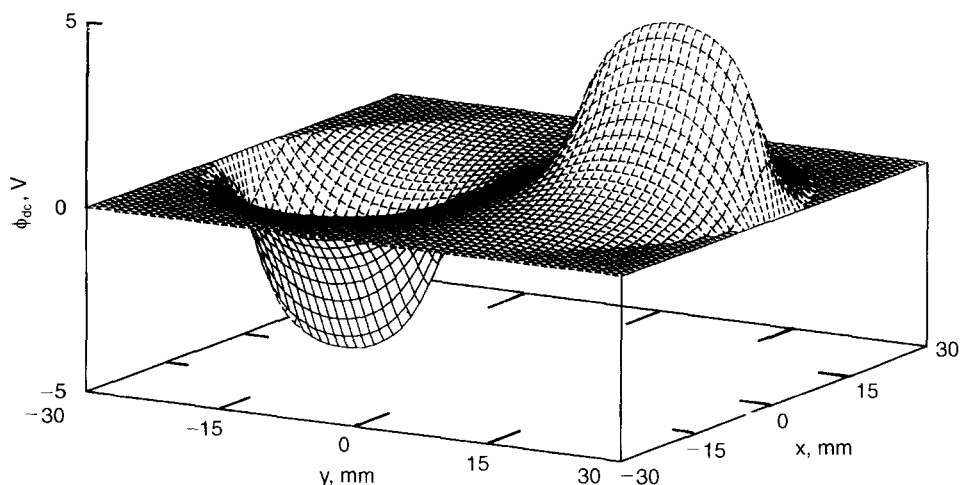


Fig. 12. The dc potential distribution at the midplane ($z = 0$).

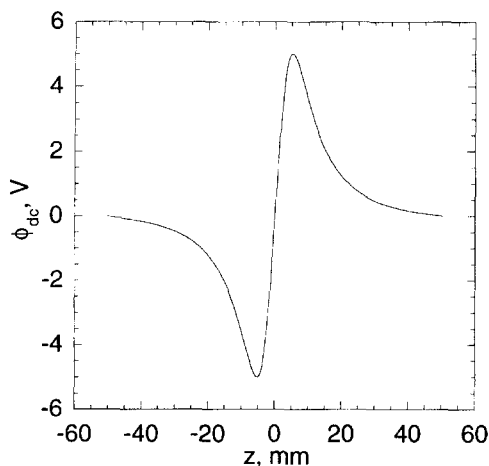


Fig. 13. The dc potential distribution as a function of z on the axis of the chamber ($r = 0$).

is $C_0 = 0.437$, which is in very good agreement with the value 0.441 ± 0.014 based on single particle levitation experiments.

CONCLUSIONS

A new experimental technique has been presented which employs the levitation of two-particle arrays to characterize the electric field and particle dynamics associated with a double-ring electrodynamic balance. This two-particle method agrees with theoretical computations in that the r -component of the electric field is a linear function of the radius for $r/R < 0.3$. In addition, direct measurement of the levitation strength constant C_0 has been reported for the first time for a double-ring balance, and the distortion of the electric field by mounting posts attached to the rings has been demonstrated by solving Laplace's equation for a non-axisymmetric geometry.

Table 1 presents a summary of the findings of this study. There is good agreement between all C_0 values obtained, although the ring charge simulation technique is limited to axisymmetric electrodes. In addition, there is reasonable agreement between C_1 values obtained by all of the techniques except the method requiring measurement of the amplitude of particle oscillation. As shown in Table 1, the ratio C_1/C_0 obtained by marginal

Table 1. Comparison of C_1 and C_0 values obtained in this study

Technique		Measured				Predicted		
		Point method	Delta method	Equation of motion	Single particle	Marginal stability	Charge simulation	Laplace's equation
Results	C_0	—	—	—	0.441	—	0.410	0.437
	C_1	0.0365	0.111	0.0357	—	0.0309*	—	0.032(⊥) 0.043(∥)
	C_1/C_0	—	—	—	—	0.070	—	0.073(⊥) 0.098(∥)

* C_1 based on the measured values of C_0 and C_1/C_0 .

stability (or springpoint) measurements is in good agreement with the ratio determined from the values of $C_{1\perp}$ and C_0 computed by solving Laplace's equation for the asymmetrical system.

Acknowledgements—This work was made possible through an exchange program sponsored by the National Science Foundation (Grant Number INT-9513934) and the Deutscher Akademischer Austauschdienst (DAAD). The authors would also like to thank the National Science Foundation for additional support through Grant CTS-9528897, and they acknowledge the assistance of Professor Marcia B. Baker, Li-Jen Chen and Dr. David S. Covert.

REFERENCES

- Abramowitz, M. and Stegun, I. A. (1972) *Handbook of Mathematical Functions with Formulas, Graphs and Mathematical Tables*. Dover, New York.
- Arnold, S. and Folan, L. M. (1987) Spherical void electrodynamic levitator. *Rev. Sci. Instrum.* **58**, 1732.
- Arnold, S. and Hessel, N. (1985) Photoemission from single electrodynamically levitated microparticles. *Rev. Sci. Instrum.* **56**, 2066.
- Berglund, R. N. and Liu, B. Y. H. (1973) Generation of monodisperse aerosol standards. *Envir. Sci. Technol.* **7**, 147.
- Bohren, C. F. and Huffman, D. R. (1983) *Absorption and Scattering of Light by Small Particles*. Wiley-Interscience, New York.
- Davis, E. J. (1985) Electrodynamic balance stability characteristics and application to the study of aerocolloidal particles. *Langmuir* **1**, 379.
- Davis, E. J. (1992) Microchemical engineering: the physics and chemistry of the microparticle. In *Advances in Chemical Engineering*, Vol. 18, Academic Press, Boston.
- Davis, E. J. and Bridges, M. A. (1994) The Rayleigh limit of charge revisited: light scattering from exploding droplets. *J. Aerosol Sci.* **25**, 1271.
- Davis, E. J., Buehler, M. F. and Ward, T. L. (1990) The double-ring electrodynamic balance for microparticle characterization. *Rev. Sci. Instrum.* **61**, 1281.
- Frickel, R. H., Shaffer, R. E. and Stamatoff, J. B. (1978) Chambers for the electrodynamic trapping of charged aerosol particles. Report No. ARCSL-TR-77041, Chemical Systems Laboratory, Aberdeen Proving Ground, MD.
- Hartung, W. H. and Avedisian, C. T. (1992) On the electrodynamic balance. *Proc. Roy. Soc. Lond. A* **437**, 237.
- Loyalka, S. K., Tekasakul, P., Tompson, R. V. and Warder, R. C. (1995) Computation of electric fields and particle motion in electrodynamic balances. *J. Aerosol Sci.* **26**, 445.
- Müller, A. (1960) Theoretische untersuchungen über das verhalten geladener teilchen in sattelpunkten elektrischer wechselfelder. *Ann. Physik* **6**, 206.
- Paul, W. and Steinwedel, H. (1953) Quadrupole mass filter. *Z. Naturforsch. A* **8**, 488.
- Reischl, G., John, W. and Devor, W. (1997) Uniform electrical charging of monodisperse aerosols. *J. Aerosol Sci.* **8**, 55.
- Reist, P. C. (1984) *Introduction to Aerosol Science*. Macmillan, New York.
- Richardson, C. B. and Spann, J. F. (1984) Measurement of the water cycle in a levitated ammonium sulfate particle. *J. Aerosol Sci.* **15**, 563.
- Sloane, C. S. and Elmoursi, A. A. (1987) Characterization of an electrodynamic balance for suspending charged droplets. In *Conference Record of the IEEE Industry Applications Meeting*. Part II, p. 1568. IEEE, New York.
- Straubel, H. (1955) Zum Öltröpfchenversuch von Millikan. *Die Naturwissenschaften* **42**, 506.
- Straubel, H. (1956) Die Dosierung von Substanzmengen unter 10^{-6} g mittels elektrostatischer Aufladung für Elektrochemie. *Zeit. Elektrochem.* **60**, 1033.
- Tian, Y. and Apfel, R. E. (1996) A novel multiple drop levitator for the study of drop arrays. *J. Aerosol Sci.* **27**, 721.
- Vehring, R., Aardahl, C. L., Davis, E. J., Schweiger, G. and Covert, D. S. (1997) Electrodynamic trapping and manipulation of particle clouds. *Rev. Sci. Instrum.* **68**, 70.
- Wuerker, R. F., Shelton, H. and Langmuir, R. V. (1959) Electrodynamic containment of charged particles. *J. Appl. Phys.* **30**, 342.